Structural and Diffusional Effects of Hydrogen in TiNi

Alan R. Pelton, Christine Trépanier, Xiao-Yan Gong, Andreas Wick and Katherine C. Chen

Proceedings of SMST-2003, Monterey, CA, eds., A.R. Pelton and T.W. Duerig, 33-42 (2004)

2004

SMST-2003

Proceedings of the International Conference on

Shape Memory and Superelastic Technologies

5 May to 8 May 2003
Asilomar Conference Center
Pacific Grove, California, USA

Editors
Alan R. Pelton
Tom Duerig

Published by:
SMST Society, Inc.
c/o SRI M/S AA287
333 Ravenswood Avenue
Menlo Park, California 94025
USA
Telephone: (650) 879-6476
E-mail: info@smst.org
Website: www.smst.org

Copies of this book may be ordered through the SMST website at *www.smst.org* or by calling the SMST office at (650) 859-6476, or through ASM International, Customer Service at (440) 338 5151 x5537 or at *www.asminternational.org*.

Printed and bound in the United States of America

Library of Congress Control Number: 2004102781

Publisher's Cataloging in Publication Data
SMST-2003: proceedings of the international conference on shape memory and superelastic technologies / edited by Alan R. Pelton and Tom Duerig.
xvi; 746 p.; 26 cm
Includes bibliographical references and index.
ISBN 0-9660508-3-5
1. Alloys—Congresses. 2. Alloys—Thermomechanical properties. 3. Shape memory effect. I. Pelton, Alan (Alan R.) II. Duerig, Tom (Thomas W.)

TN690.S675 2004
669'.94—dc20

***
Production Services by TIPS Technical Publishing, Inc.

STRUCTURAL AND DIFFUSIONAL EFFECTS OF HYDROGEN IN TINI

Alan R. Pelton,[1] Christine Trépanier,[1] Xiao-Yan Gong,[1]
Andreas Wick,[1] and Katherine C. Chen[2]

[1]Nitinol Devices & Components, 47533 Westinghouse Dr., Fremont, CA 94539
[2]Department of Materials Engineering, California Polytechnic State University, San Luis Obispo, CA 93407

ABSTRACT

Hydrogen can be inadvertently added to Nitinol medical devices through electropolishing, caustic cleaning, or exposure to other acidic or basic solutions. Moderately high hydrogen concentrations can lead to embrittlement characterized by lowered ductility and changes in transformation behavior. The purpose of the present paper is to discuss recent results on the effects of hydrogen in annealed TiNi. Samples are charged with hydrogen and analyzed with X-ray diffraction (CXRD); these data indicate that even relatively small amounts of hydrogen can affect the crystal structure. Additions of up to 1000 wppm hydrogen increase the atomic volume by more than 2%, decrease peak intensity and broaden peak width. These observations are consistent with hydrogen-induced lattice strain. Peak splitting and additional diffraction peaks are observed with the absorption of 6000 wppm hydrogen, which indicates formation of a new phase. It is speculated that the new phase may be based on the B2 structure or may be stress-induced R-phase or martensite. This paper also discusses experiments and analysis on the removal of hydrogen from TiNi wire with 800 wppm through heat treatments at 400 to 800°C for 30 to 3000 seconds. Extensive experimental and analytical computations show that the activation energy of hydrogen diffusion under these conditions is approximately 125 kJ/mol.

KEYWORDS

Nitinol, Hydrogen, Heat Treatment, Kinetics, Phase Transformation, Embrittlement, Diffusion, X-ray Diffraction

INTRODUCTION

TiNi medical devices are often subjected to processing conditions that could lead to high concentrations of hydrogen, such as cathodic cleaning with NaOH, acid etching, electropolishing in acids, or heat treatments in hydrogen-containing gas. At high enough concentrations (~100 wppm = 0.01 wt.%

~ 0.5 at.%), hydrogen embrittlement is observed, similar to other titanium-based alloys [1]. The main hydrogen effects observed in TiNi include reduced ductility [2,3], loss of shape memory properties [2], and shorter fatigue life [4]. However, there is still a general lack of understanding of the interactions between TiNi and hydrogen and how these interactions may affect processing and properties, especially of medical devices. To date, the majority of technical investigations of the TiNi-H and related systems have focused on phase equilibria in alloys with unreported actual compositions and transformation temperatures. However, a brief summary of these articles is provided in the background section below in order to put the present results into better context. The purpose of this report therefore is to summarize a series of experiments that use X-ray Diffraction to monitor structural effects in TiNi as a function of hydrogen concentration. In addition, this report will quantify the desorption kinetics from thermal treatments on hydrogen-charged TiNi.

BACKGROUND: TINI-H PHASE EQUILIBRIA AND STRUCTURES

Burch and Mason investigated the solubility relationships of hydrogen in binary TiNi with partial pressures in the range of 0.005 to 2 MPa and temperatures of 52 to 427° C [5–7]. Their results indicate that hydrogen is absorbed in TiNi in a continuous solid solution up to maximum hydrogen concentration of 40 at.% or 13000 wppm ($TiNiH_{1.4}$) without hydride formation. Schmidt *et al*. [8,9] investigated hydrogen solubility in TiNi for high temperatures (500–950° C) and low pressures (<0.1 MPa) up to a maximum concentration of approximately 500 wppm. They found that the solubility *decreases* with increasing temperature, but that the solubility is linear with the square root of hydrogen pressure; this behavior follows Sievert's Law. Yamanaka et al. [10] observed the interstitial $TiNiH_{1.4}$ phase below 270° C, whereas above about 500° C and a hydrogen pressure of ~13 MPa the authors suggest that TiNi decomposes into $TiNi_3$ + TiH_2.

Buchner et al. [11] investigated the structural effects of absorbed hydrogen in TiNi from X-ray diffraction studies, and found that the lattice parameter of the B2 structure increased from 3.01 to 3.10 Å, which corresponds to a volume increase of nearly 10%. They proposed a TiNiH stoichiometric phase (33 at.% or about 9400 wppm hydrogen) corresponding to an 8 × 8 × 8 B2 structure with a = 24.8 Å. Wu *et al*. [12,13] observed extra 1/2 diffraction reflections in TiNi-H by transmission electron microscopy and proposed that they were due to hydrogen ordering on octahedral sites associated with the Ti sublattice. Analysis of their diffraction data suggests a superlattice with the hydrogen occupying only O_y and O_z sites that produces a 4 × 2 × 2 tetragonal structure with a = 3.0 Å and b = c = 3.1 Å.

Equiatomic TiCo and TiFe are isostructural with B2 TiNi, yet both systems show dramatically different behavior with hydrogen additions. The maximum solubility of hydrogen in the TiCo B2 structure equates to 5 at.% or about 950 wppm [7]. The β-phase hydride has 30at.% (7850 wppm) hydrogen with a tetragonal structure with a = b = 6.14 Å and c = 9.06 Å, which is approximately a 2 by 2 by 3 unit cell based on the hydrogen-free B2 cell structure. At temperatures above 202° C, hydrogen is continuously absorbed in the α-phase without formation of β. Phase equilibria in the TiFe-H system is better understood due to the extensive research on potential hydrogen storage applications. Wenzel [14] presented a theoretical pseudobinary TiFe-H phase diagram based on data from several researchers. This proposed phase diagram shows a large two-phase α +β region, where the maximum solubility of hydrogen in the α phase is $TiFeH_{0.04}$ (~ 400 wppm) at about 200° C [15]. Neutron diffraction studies [16] of the α-$FeTiD_{0.04}$ phase show that with Fe at 000 and Ti at in $\frac{1}{2}\frac{1}{2}\frac{1}{2}$ the B2 structure, deuterium randomly occupies octahedral positions at

$\frac{1}{2}00,\ 0\frac{1}{2}0,\ and\ 00\frac{1}{2}$, midway between the Fe atoms. Hydrogen atoms also occupy octahedral sites in the β-FeTiH phase to form an orthorhombic unit cell [14].

EXPERIMENTAL MATERIALS AND METHODS

Two sets of experiments were performed on annealed and hydrogen-charged $Ti_{49.2}Ni_{50.8}$ for XRD studies. Hydrogen analyses were obtained with the vacuum fusion test method from Luvak, Inc. (Boylston, Mass.). In the first set of experiments, 0.4 mm diameter wires were mechanically and chemically polished prior to H_3PO_4 exposure at 90° C for 1 min. (182 wppm hydrogen), 5 min. (583 wppm hydrogen), 10 min. (1050 wppm hydrogen), and 20 min. (6028 wppm hydrogen). In the second experiments, 12.7 mm diameter discs were cut into 1 mm thick sections, annealed, mechanically polished, and electropolished. They were then immersed in H_3PO_4 at 90° C for 30 min. to obtain an estimated >5000 wppm hydrogen. XRD analyses were performed on these wires and discs on a Siemens Kristalloflex D5000 diffractometer with 40 kV Cu Kα radiation with a Ni filter. Data were obtained at 0.01 increments from 10–90 2θ at a scan rate of 0.5/min.

Another set of experiments was done on annealed 1.0 mm diameter wires that were mechanically polished and electropolished prior to immersing in H_3PO_4 at 90° C for 40 min. (800 wppm). These samples were then heat treated in air at 400–800° C in 100° C increments for 30, 100, 300, 1000, and 3000 seconds and analyzed for hydrogen content to determine diffusion behavior. In addition, a length of this hydrogen-charged wire was centerless ground in increments of approximately 0.015 mm until a diameter of 0.8 mm was reached. The wire was then ground in increments of 0.025 mm to a final diameter of 0.63 mm. Sections of these wires were cut after each diameter reduction and analyzed to determine the residual hydrogen absorption profile.

RESULTS AND DISCUSSION

X-Ray Diffraction

Figure 1 shows the XRD patterns of the hydrogen-charged 0.4 mm wires between 35 and 50 2θ. The patterns illustrate that the $\{110\}_{B2}$ peak shifts to lower angles with a corresponding lattice parameter increase from 3.025 to 3.047 Å (2.2% volume increase) with an increase in hydrogen from 20 to 1050 wppm. In addition, as the hydrogen content increases, the $\{110\}_{B2}$ peaks become broader with lower peak intensity and with the onset of peak splitting. Extra peaks also emerge at 38.3, 39.8, and 45 2θ. With 6028 wppm hydrogen, there are additional peaks at 38.5 and 45.3 and the $\{110\}_{B2}$ peak has split into two diffuse, lower intensity peaks.

In order to minimize wire textural effects on the XRD patterns, annealed and hydrogen-charged TiNi discs with 100 μm grain size were also analyzed. Results from these scans are shown in Figure 2 demonstrate dramatic hydrogen-induced structural changes. The pattern from the annealed sample is consistent with the expected B2 structure and the three major peaks were analyzed as follows: 42.5 2θ $\{110\}_{B2}$, 52.7 2θ $\{111\}_{B2}$, and 77.6 2θ $\{211\}_{B2}$. The calculated lattice parameter based on the $\{211\}_{B2}$ peak is 3.01 Å. The XRD pattern from the hydrogen-charged disc contains several new peaks, which are compared to hydride structures in Table 1. The Buchner et al. [11] data shown in this table do not extend to lower angles, so it is not possible to determine if their large B2 structure matches the present pattern. The largest planar spacing in the Wu *et al*. tetragonal structure is 3.10 Å [12,13], which is inconsistent with the 4.70Å plane observed in Figure 2. The

Table 1 Diffraction Peaks and Corresponding Planar Spacings from Figure 2 and Literature Data

Figure 2		Buchner et al. [11]		Wu et al. [12,13]		Burch and Mason [7]	
Angle (2θ)	**d (Å)**	**Angle (2θ)**	**d (Å)**	**Angle (2θ)**	**d (Å)**	**Angle (2θ)**	**d (Å)**
18.9	4.70					19.60	4.53
37.85	2.38						
38.35	2.35	39	2.31			39.80	2.27
41.65	2.17	41	2.20	41.19	2.19	41.61	2.17
42.3	2.14			41.91	2.16		
45.0	2.01	44.4	2.04			45.16	2.01
77.15	1.24	75	1.27	75.56	1.26	77.78	1.23

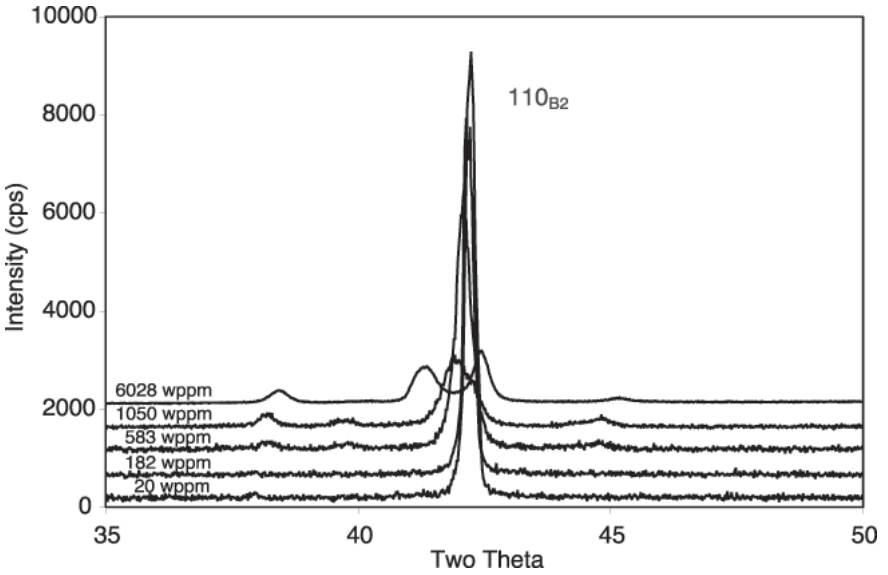

Figure 1 XRD patterns of annealed and hydrogenated $Ti_{49.2}Ni_{50.8}$ wires. Note the dramatic change in position and intensity of the diffraction peaks near 42 2θ with increased hydrogen.

CoTi-H-type structure [7] has a large unit cell and therefore has a number of possible matching peaks, but the fit was not promising. Cheng *et al*. [17] (not included in Table 1) observed similar patterns to Figure 2 and conclude that the hydride is based on a B2 cell, but they did not further analyze the atomic structure.

The data in Figures 1 and 2 are consistent with hydrogen-induced lattice strain, as illustrated with an increase in the B2 lattice parameter as well as the decrease in peak intensity and broadened peaks [18]. Furthermore, in contrast to the experiments by Burch and Mason [5–7], it appears that

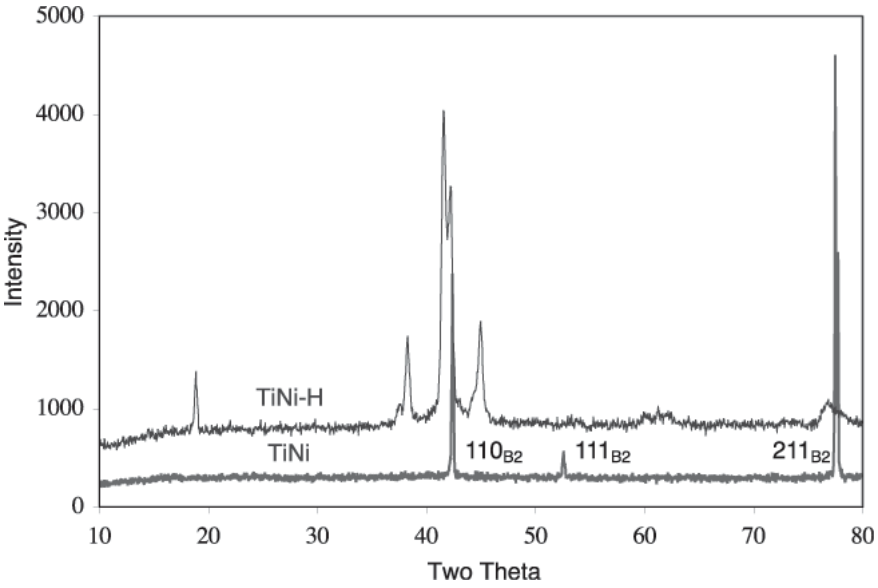

Figure 2 X-ray diffraction patterns of annealed (TiNi) and hydrogenated (TiNi-H) $Ti_{49.2}Ni_{50.8}$ discs. The three major peaks are identified for TiNi.

hydrogen additions to TiNi lead to new phase(s) under the present experimental conditions. Although the current data do not directly match with the cubic or tetragonal structures cited above from the literature, it is likely that hydrogen occupies octahedral sites (as found in TiFe-H [16]), thus forming structures based on the B2 lattice. Alternatively, since the A_f of the fully annealed discs and wire is approximately –20° C, the internal stresses caused by hydrogen-induced atomic volume increase could trigger transformations to R-phase or martensite. Some of the peaks in the hydrogen-charged sample in Figure 2, namely 18.9, 37.85, 38.35, and 45, are consistent with B19' martensite [19–21], especially given that there is still disagreement on the exact martensitic structure. Furthermore, the two peaks at 41.65 and 42.3 are consistent with peak splitting associated with R-phase formation [22,23]. However, this hydrogen-induced transformation explanation is quite speculative at the present time.

Hydrogen Diffusion in Nitinol

Figure 3 shows the residual hydrogen concentration profile in the centerless ground TiNi wire. These data demonstrate that the hydrogen concentrates at the surface of the wire, with a steep gradient between 0.9 mm and 0.85 mm, and then levels off to approximately 250 wppm at 0.63 mm diameter. Wires with this initial hydrogen profile were heat treated in air as described above and analyzed for the hydrogen concentration. Figure 4 shows the hydrogen concentration as a function of time and temperature after these heat treatments. These results illustrate that air heat treatments are effective in reducing hydrogen from the samples. The rate of hydrogen desorption from the Nitinol wire can be estimated by considering a one-dimensional solution to Fick's Second Law [24]:

$$\frac{\partial C}{\partial t} = D\left[\frac{\partial^2 C}{\partial r^2} + \frac{1}{r}\frac{\partial C}{\partial r}\right] \tag{1}$$

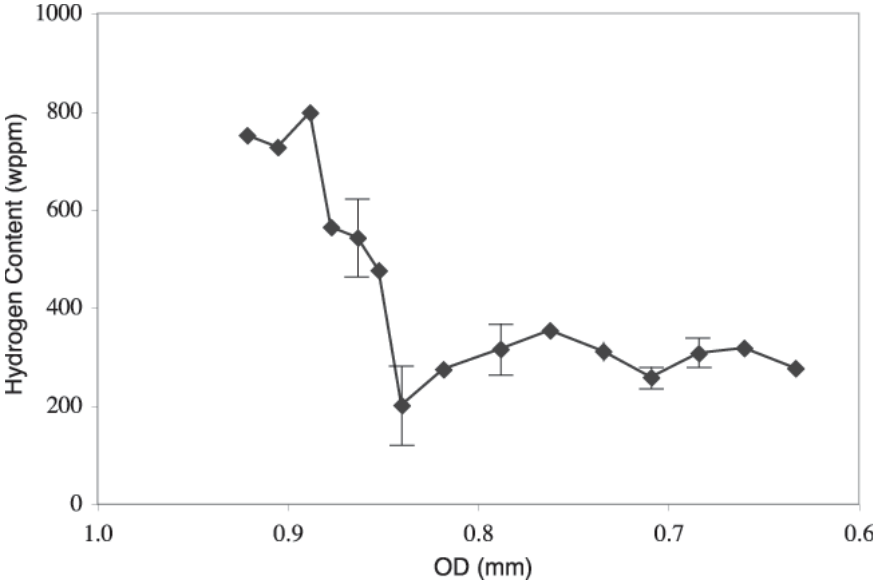

Figure 3 Residual hydrogen concentration of the ground $Ti_{49.2}Ni_{50.8}$ wire used for diffusion studies.

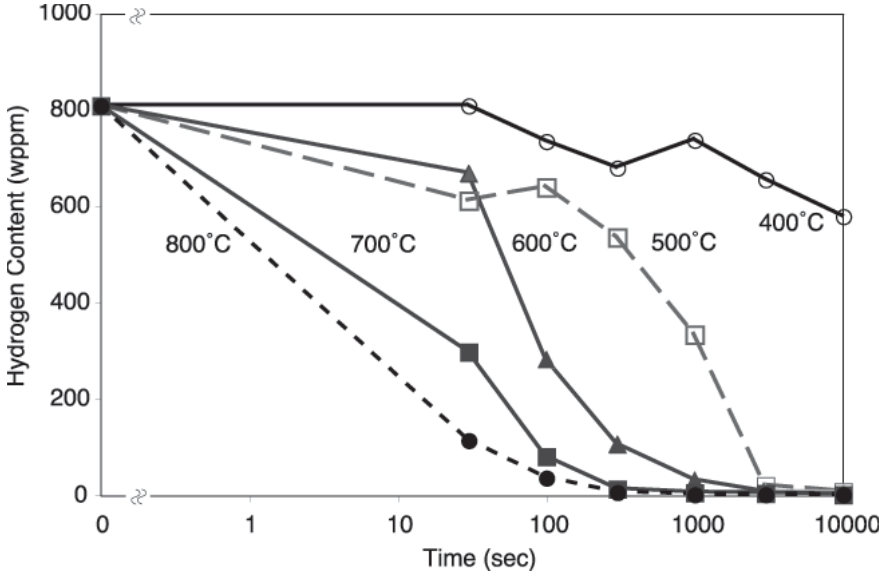

Figure 4 Effect of time and temperature on the hydrogen concentration of $Ti_{49.2}Ni_{50.8}$ wire with the initial profile shown in Figure 3.

where C is hydrogen composition, t is time, and r is the radius of a cylinder. Textbooks offer standard methods to solve this second-order partial differential equation when the concentration profile is known. However, since it is not possible to cut the wires into radial sections to determine the concentration in each segment, a different analytical approach was taken. For the present case, the *residual* composition was measured in each wire section after each thermal treatment. The resulting composition profile can then be analyzed to determine the actual concentrations as follows [25]:

$$C_t = C_0 - \frac{2C_0}{a}\sum_{n=1}^{\infty}\frac{J_0(r\alpha_n)}{\alpha_n J_1(a\alpha_n)}\exp(-D\alpha_n^2 t_0). \tag{2}$$

where $a\alpha_n$ satisfies $J_0(a\alpha_n) = 0$, and a is the wire outer radius. J_0 and J_1 are the zero and the first-order Bessel functions of first kind, respectively. C_0 is the environmental hydrogen concentration that can be determined through curve fitting. Integration of the above equation provides the total (averaged) residual concentration at the radii, r:

$$C_r = C_0 - \frac{4C_0 a}{r}\sum_{n=1}^{\infty}\frac{J_1(r\alpha_n)}{(a\alpha_n)^2 J_1(a\alpha_n)}\exp(-D\alpha_n^2 t_0). \tag{3}$$

Equation 3 is then used to analyze the hydrogen-concentration data for each wire radius. From this data set, the quantity $D\alpha_n^2 t_0$ in equation 2 can be determined and, therefore, the hydrogen concentration at any position in the wire is known. Once C_0 and $D\alpha_n^2 t_0$ are known, equation 2 provides the initial hydrogen concentration profile. Therefore, at any time during the diffusion anneals, the hydrogen concentration can be written as

$$C_t = C_a\sum_{n=1}^{\infty}\frac{4}{(a\alpha_n)^2}\exp(-D\alpha_n^2 t)\left[1-\exp(-D\alpha_n^2 t_0)\right]. \tag{4}$$

We can solve equation 4 for the diffusivity, D, at each temperature as summarized in Table 2. Diffusion rates generally follow an Arrhenius equation where the activation energy and pre-exponential factors are determined by plotting the data in Table 2 in the form of ln D *vs* 1/T as shown in Figure 5. From this graph, the activation energy is calculated from the slope to be 124.9 kJ/mol and the intercept, D_o is 15.1 cm^2/sec. Hydrogen diffusivity in these Nitinol wires can therefore be summarized as

$$D = 15.1\exp\left[-\frac{124.9\,kJ/mol}{RT}\right]$$

The activation energy determined from the wires is considerably higher than calculated by Schmidt et al. [8,9] of 46.2 kJ/mol in TiNi cylinders that contain less than 500 wppm hydrogen. These authors conducted their absorption experiments under controlled partial pressures of hydrogen in an UHV system between 500° C and 950° C so that only bulk diffusion mechanisms were measured. Furthermore, their samples were sputter coated with 1–2 μm thick palladium in order to minimize surface effects during absorption.

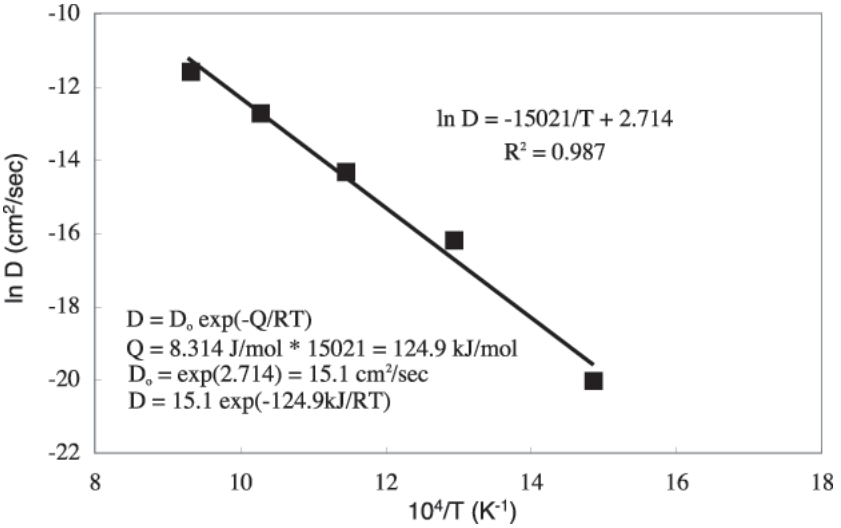

Figure 5 Diffusivity of hydrogen in $Ti_{49.2}Ni_{50.8}$ wires with an initial hydrogen content of 800 wppm based on the data shown in Figure 4 and from Table 2.

Table 2 Diffusivity of Hydrogen in TiNi as a Function of Temperature

Temperature (C)	Diffusivity (cm^2/sec)
400	2.02×10^{-9}
500	9.32×10^{-8}
600	6.07×10^{-7}
700	3.01×10^{-6}
800	9.31×10^{-6}

Similarly, a 47.8 kJ/mol hydrogen activation energy was measured from diffusion experiments on $Ti_{49.2}Ni_{50.8}$ tubing with approximately 100 wppm hydrogen [26]. This tubing was equilibrated at 700° C in a high partial pressure of argon after hydrogen absorption, which resulted in a more uniform initial hydrogen profile than observed in Figure 3. Desorption kinetics were obtained after diffusion anneals between 400° C and 900° C [26]. Under these conditions, therefore, hydrogen desorption closely followed the bulk diffusion behavior reported by Schmidt et al. [8,9].

The present diffusion experiments were carried out under conditions that simulate possible hydrogen contamination during medical device manufacturing, such as exposure to acids at relatively low temperatures. The hydrogen profile data shown in Figure 3 indicate that there is a high accumulation of hydrogen at the surface of the samples with a steep concentration gradient towards the center of the wire. It is clear that the low temperature, short time exposure to the H_3PO_4 was insufficient to diffuse the hydrogen long distances in the wire. Furthermore, the XRD patterns in Figures 1 and 2 demonstrate that these high levels of hydrogen at the surface lead to hydride formation or possibly

hydrogen-stabilized martensitic transformations as discussed above. As such, the hydrogen is effectively trapped in these new phases require higher energies to dissociate and then diffuse out of the sample during heat treatments. The complex surface oxides [27] that form during the diffusion anneals may also influence the diffusion rate.

CONCLUSION

This study investigated structural and diffusional effects of hydrogen in annealed and hydrogen-charged TiNi wires and discs. The following observations were made from the XRD studies:

1. The $\{110\}_{B2}$ peaks shift to lower angles with a corresponding increase in lattice parameter from 3.025 to 3.047 Å (2.2% volume increase) and decrease in peak intensity as hydrogen increases from 20 to 1050 wppm. These effects are consistent with internal stresses caused by the absorbed hydrogen. Additional diffraction peaks and splitting of the $\{110\}_{B2}$ peak are also observed with this increased hydrogen content.

2. With 6028 wppm hydrogen, the $\{110\}_{B2}$ peak split into two diffuse, lower intensity peaks with formation of extra diffraction peaks. These observations are likely due to ordering of the hydrogen atoms on octahedral sites to form a structure based on the B2 lattice. An alternative explanation is that hydrogen could trigger stress-induced R-phase or martensite transformations.

Annealed TiNi wires with 800 wppm hydrogen were profiled and analyzed for diffusion desorption in the temperature range of 400 to 800° C for times of 30 to 3000 seconds. The residual hydrogen values were analyzed to obtain a diffusion activation energy of 124.9 kJ/mol. It is speculated that this large activation energy may be due to effects of surface hydrogen phases formed during the low-temperature hydrogen absorption. The hydrogen-diffusion equation may be used to estimate temperatures and times to remove hydrogen contamination from TiNi alloys.

REFERENCES

1. A.W. Thompson and N.R. Moody, eds., *Hydrogen Effects in Materials* (Warrendale, Pa: TMS, 1996), p. 699.

2. B.L. Pelton, T. Slater, and A.R. Pelton, in *SMST-97: Proceedings of the Second International Conference on Shape Memory and Superelastic Technologies,* eds. A Pelton et al. (Pacific Grove, Calif.: International Organization on SMST), p. 395.

3. T. Asaoko, H. Saito, and Y. Ishida, in *Proc. ICOMAT (*1993), p. 1003.

4. K. Yokoyama *et al.*, *Biomaterials* **22** (2001), p. 2257.

5. R. Burch and N.B. Mason, *J.C.S. Faraday I* **75** (1979), p. 561.

6. R. Burch and N.B. Mason, *J.C.S. Faraday I* **75** (1979), p. 578.

7. R. Burch and N.B. Mason, *Z. Physikkalische Chemie Neue Folge* **116** (1979), p. 185.

8. R. Schmidt *et al.*, *J. Phys.: Condens. Matter* **I** (1989), p. 2473.

9. R. Schmidt, M. Schlereth, and H. Wipf, *Z. Physikkalische Chemie Neue Folge* **164** (1989), p. 803.

10. K. Yamanaka, H. Saito, and M. Someno, *Nippon Kagaku Kaishi* **8** (1975), p. 1267.

11. H. Buchner *et al.*, *Z. Metallkunde* **63** (1972), p. 497.

12. S.K. Wu and C.M. Wayman, *Acta metall.* **36** (1988), p. 1005.

13. S.K. Wu, A.G. Khachaturyan, and C.M. Wayman, *Acta metall.* **36 (**1988), p. 2065.

14. H. Wenzel, *J. Less Common Metals* **74** (1980), p. 351.

15. J.-M. Welter, G. Arnold, and H. Wenzel, *J. Phys. F: Met. Phys.* **13** (1983), p. 1773.

16. P. Thompson *et al.*, *J. Phys. F: Metal Phys.* **10** (1980), p. L57.

17. F.T Cheng, P. Chi, and H.C. Man, *Scripta Mater.* **47** (2002), p. 89.

18. B.D. Cullity, *Elements of X-Ray Diffraction* (Addison-Wesley, 1956), p. 431.

19. K. Otsuka, T. Sawamura, and T. Shimizu, *Phys. Status Solidi* **A5** (1971), p. 457.

20. G. Michal and R. Sinclair, *Acta Cryst Sec B.* **37** (1981), p. 1803.

21. W. Bührer *et al.*, *J. of Phys. F: Metal Physics* **13F** (1983), p. L77.

22. H.C. Ling and R. Kaplow, *Metall. Trans.* **12A** (1981), p. 2101.

23. V. Imbeni *et al.*, in *SMST-2003: Proceedings of the International Conference on Shape Memory and Superelastic Technologies*, eds. A.R. Pelton and T. Duerig (Pacific Grove, Calif.: International Organization on SMST).

24. P. G. Shewmon, *Diffusion in Solids* (New York: McGraw-Hill Book Company).

25. J. Crank, *The Mathematics of Diffusion* (Oxford: Clarendon Press,1975).

26. A.R. Pelton *et al.* (unpublished research, 2002).

27. L. Zhu, J.M. Fino, and A.R. Pelton, in *SMST-2003: Proceedings of the International Conference on Shape Memory and Superelastic Technologies*, eds. A.R. Pelton and T. Duerig (Pacific Grove, Calif.: International Organization on SMST).